New Journal of Physics
The open access journal at the forefront of physics
Deutsche Physikalische Gesellschaft DPG | IOP Institute of Physics

LHC optics measurement with proton tracks detected by the Roman pots of the TOTEM experiment

The TOTEM Collaboration

G Antchev[12], P Aspell[8], I Atanassov[8,12], V Avati[8], J Baechler[8], V Berardi[5a,5b], M Berretti[7b], E Bossini[7b], U Bottigli[7b], M Bozzo[6a,6b], E Brücken[3a,3b], A Buzzo[6a], F S Cafagna[5a], M G Catanesi[5a], C Covault[9], M Csanád[4,13], T Csörgö[4], M Deile[8], M Doubek[1b], K Eggert[9], V Eremin[14], F Ferro[6a], A Fiergolski[5a,15], F Garcia[3a], V Georgiev[11], S Giani[8], L Grzanka[10,16], J Hammerbauer[11], J Heino[3a], T Hilden[3a,3b], A Karev[8], J Kašpar[1a,8], J Kopal[1a,8], V Kundrát[1a], S Lami[7a], G Latino[7b], R Lauhakangas[3a], T Leszko[15], E Lippmaa[2], J Lippmaa[2], M V Lokajíček[1a], L Losurdo[7b], M Lo Vetere[6a,6b], F Lucas Rodríguez[8], M Macri[6a], T Mäki[3a], A Mercadante[5a], N Minafra[5b,8], S Minutoli[6a], F Nemes[4,13], H Niewiadomski[8], E Oliveri[7b], F Oljemark[3a,3b], R Orava[3a,3b], M Oriunno[17], K Österberg[3a,3b], P Palazzi[7b], Z Peroutka[11], J Procházka[1a], M Quinto[5a,5b], E Radermacher[8], E Radicioni[5a], F Ravotti[8], E Robutti[6a], L Ropelewski[8], G Ruggiero[8], H Saarikko[3a,3b], A Scribano[7b], J Smajek[8], W Snoeys[8], J Sziklai[4], C Taylor[9], N Turini[7b], V Vacek[1b], J Welti[3a,3b], J Whitmore[18], P Wyszkowski[10] and K Zielinski[10]

[1a] Institute of Physics, ASCR, Praha, Czech Republic
[1b] Czech Technical University, Praha, Czech Republic
[2] National Institute of Chemical Physics and Biophysics NICPB, Tallinn, Estonia
[3a] Helsinki Institute of Physics, Helsinki, Finland
[3b] Department of Physics, University of Helsinki, Helsinki, Finland
[4] MTA Wigner Research Center, RMKI Budapest, Hungary
[5a] INFN Sezione di Bari, Bari, Italy
[5b] Dipartimento Interateneo di Fisica di Bari, Italy
[6a] INFN Sezione di Genova, Genova, Italy
[6b] Università degli Studi di Genova, Genova, Italy
[7a] INFN Sezione di Pisa, Pisa, Italy
[7b] Università degli Studi di Siena and Gruppo Collegato INFN di Siena, Siena, Italy
[8] CERN, Geneva, Switzerland
[9] Case Western Reserve University, Dept. of Physics, Cleveland, OH, USA
[10] AGH University of Science and Technology, Krakow, Poland
[11] University of West Bohemia, Pilsen, Czech Republic
[12] INRNE-BAS, Institute for Nuclear Research and Nuclear Energy, Bulgarian Academy of Sciences, Sofia, Bulgaria
[13] Department of Atomic Physics, Eötvös University, Budapest, Hungary
[14] Ioffe Physical—Technical Institute of Russian Academy of Sciences, St. Petersburg, Russia
[15] Warsaw University of Technology, Warsaw, Poland
[16] Institute of Nuclear Physics, Polish Academy of Science, Cracow, Poland
[17] SLAC National Accelerator Laboratory, Stanford CA, USA

1367-2630/14/103041+19$33.00

[18] Penn State University, Dept. of Physics, University Park, PA, USA
E-mail: frigyes.janos.nemes@cern.ch

Received 13 June 2014, revised 26 July 2014
Accepted for publication 18 August 2014
Published 28 October 2014
New Journal of Physics **16** (2014) 103041
doi:10.1088/1367-2630/16/10/103041

Abstract

Precise knowledge of the beam optics at the LHC is crucial to fulfill the physics goals of the TOTEM experiment, where the kinematics of the scattered protons is reconstructed with near-beam telescopes—so-called Roman pots (RP). Before being detected, the protons' trajectories are influenced by the magnetic fields of the accelerator lattice. Thus precise understanding of the proton transport is of key importance for the experiment. A novel method of optics evaluation is proposed which exploits kinematical distributions of elastically scattered protons observed in the RPs. Theoretical predictions, as well as Monte Carlo studies, show that the residual uncertainty of the optics estimation method is smaller than 2.5‰.

Keywords: elastic scattering, LHC proton transport, Roman pot, optics reconstruction, TOTEM experiment

1. Introduction

The TOTEM experiment [1] at the LHC is equipped with near beam movable insertions—called Roman pots (RP)—which host silicon detectors to detect protons scattered at the LHC interaction point 5 (IP5) [2]. This paper reports the results based on data acquired with a total of 12 RPs installed symmetrically with respect to IP5. Two units of three RPs are inserted downstream of each outgoing LHC beam: the 'near' and the 'far' unit located at $s = \pm 214.63$ m and $s = \pm 220.00$ m, respectively, where s denotes the distance from IP5. The arrangement of the RP devices along the two beams is schematically illustrated in figure 1.

Each unit consists of two vertical, so-called 'top' and 'bottom', and one horizontal RP. The two diagonals *top left of IP–bottom right of IP* and *bottom left of IP–top right of IP*, tagging elastic candidates, are used as almost independent experiments. The details of the set-up are discussed in [3].

Each RP is equipped with a telescope of ten silicon microstrip sensors of 66 μm pitch which provides a spatial track reconstruction resolution $\sigma(x, y)$ of 11 μm [4]. Given the longitudinal distance between the units of $\Delta s = 5.372$ m the proton angles are measured by the RPs with an uncertainty of 2.9 μrad.

During the measurement the detectors in the vertical and horizontal RPs overlap, which enables a precise relative alignment of all the three RPs by correlating their positions via

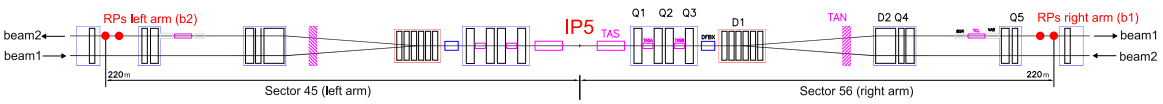

Figure 1. Schematic layout of the LHC magnet lattice at IP5 up to the 'near' and 'far' Roman pot units, where the near and far pots are indicated by full (red) dots on beams 1 and 2, at the positions indicated by arrows.

common particle tracks. An alignment uncertainty of better than 10 μm is attained, and the details are discussed in [4, 5].

The proton trajectories, thus their positions observed by RPs, are affected by the magnetic fields of the accelerator lattice. The accelerator settings define the machine optics which can be characterized with the value of β^* at IP5. It determines the physics reach of the experiment [3]: runs at high $\beta^* = 90$–2500 m are characterized by low beam divergence allowing for precise scattering angle measurements while runs of low $\beta^* = 0.5$–11 m, due to small interaction vertex size, provide higher luminosity and thus are more suitable to study rare processes. In the following sections we will analyze two representatives, the $\beta^* = 3.5$ m and 90 m optics [2, 6, 7].

In order to precisely reconstruct the scattering kinematics, an accurate model of proton transport is indispensable. TOTEM has developed a novel method to evaluate the optics of the machine by using angle-position distributions of elastically scattered protons observed in the RP detectors. The method, discussed in detail in the following sections, has been successfully applied to data samples recorded in 2010 and 2012 [8–12].

Section 2 introduces the so-called transport matrix, which describes the proton transport through the LHC lattice, while machine imperfections are discussed in section 3. The proposed novel method for optics evaluation is based on the correlations between the transport matrix elements. These correlations allow the estimation of those optical functions which are strongly correlated to measurable combinations, estimators, of transport matrix elements. Therefore, it is fundamental to study these correlations in detail, which is the subject of section 4. The applied eigenvector decomposition gives an insight into the obtainable errors of optics estimation, and provides the theoretical baseline of the method.

Section 5 brings the theory to practice, by specifying the estimators obtained from elastic track distributions measured in RPs. Finally, the applied optics estimation algorithm is discussed in section 6. The uncertainty of this novel method of LHC optics determination was estimated with Monte Carlo simulations, described in detail in section 7.

2. Proton transport model

Scattered protons are detected by the Roman pots after having traversed a segment of the LHC lattice containing 29 main and corrector magnets per beam, shown in figure 1.

The trajectory of protons produced with transverse positions[19] (x^*, y^*) and angles (Θ_x^*, Θ_y^*) at IP5 is described approximately by a linear formula

[19] The '*' superscript indicates that the value is taken at the LHC interaction point 5.

$$\vec{d}\,(s) = T\,(s) \cdot \vec{d}^{\,*}, \tag{1}$$

where $\vec{d} = (x,\ \Theta_x,\ y,\ \Theta_y,\ \Delta p/p)^T$, p and Δp denote the nominal beam momentum and the proton longitudinal momentum loss, respectively. The single pass transport matrix

$$T = \begin{pmatrix} v_x & L_x & m_{13} & m_{14} & D_x \\ \dfrac{\mathrm{d}v_x}{\mathrm{d}s} & \dfrac{\mathrm{d}L_x}{\mathrm{d}s} & m_{23} & m_{24} & \dfrac{\mathrm{d}D_x}{\mathrm{d}s} \\ m_{31} & m_{32} & v_y & L_y & D_y \\ m_{41} & m_{42} & \dfrac{\mathrm{d}v_y}{\mathrm{d}s} & \dfrac{\mathrm{d}L_y}{\mathrm{d}s} & \dfrac{\mathrm{d}D_y}{\mathrm{d}s} \\ 0 & 0 & 0 & 0 & 1 \end{pmatrix} \tag{2}$$

is defined by the optical functions [13]. The horizontal and vertical magnifications

$$v_{x,\,y} = \sqrt{\beta_{x,\,y}/\beta^*}\,\cos\Delta\mu_{x,\,y} \tag{3}$$

and the effective lengths

$$L_{x,\,y} = \sqrt{\beta_{x,\,y}\beta^*}\,\sin\Delta\mu_{x,\,y} \tag{4}$$

are functions of the betatron amplitudes $\beta_{x,\,y}$ and the relative phase advance

$$\Delta\mu_{x,\,y} = \int_{\mathrm{IP}}^{\mathrm{RP}} \frac{\mathrm{d}s}{\beta_{x,\,y}}, \tag{5}$$

and are of particular importance for proton kinematics reconstruction. The D_x and D_y elements are the horizontal and vertical dispersion, respectively.

Elastically scattered protons are relatively easy to distinguish due to their scattering angle correlations. In addition, these correlations are sensitive to the machine optics. Therefore, elastic proton-proton scattering is an ideal process to study the LHC optics.

In case of the LHC nominal optics the coupling coefficients are, by design, equal to zero

$$m_{13},\ldots,m_{42} = 0. \tag{6}$$

Also for elastically scattered protons the interaction related contribution to longitudinal momentum loss Δp is 0. However, the beam protons are characterized by a momentum spread resulting from the beam longitudinal emittance and the RF configuration. For the LHC this spread is $\delta p/p_0 = 10^{-4}$ [14], which is not significant with respect to the beam momentum offset uncertainty of 10^{-3}, reported in table 1. Therefore, the terms $D_{x,y} \times (\Delta p/p)$ and $\mathrm{d}D_{x,\,y}/\mathrm{d}s \times (\Delta p/p)$ of the transport equation (1) can be neglected in case of elastically scattered protons.

Furthermore, the horizontal phase advance $\Delta\mu_x$ is equal to π at 219.59 m (figure 2), and consequently the horizontal effective length L_x vanishes close to the far RP unit, as it is shown in figure 3. Therefore, in the proton kinematics reconstruction $\mathrm{d}L_x/\mathrm{d}s$ is used.

In summary, the kinematics of elastically scattered protons at IP5 can be reconstructed on the basis of RP proton tracks using (1)

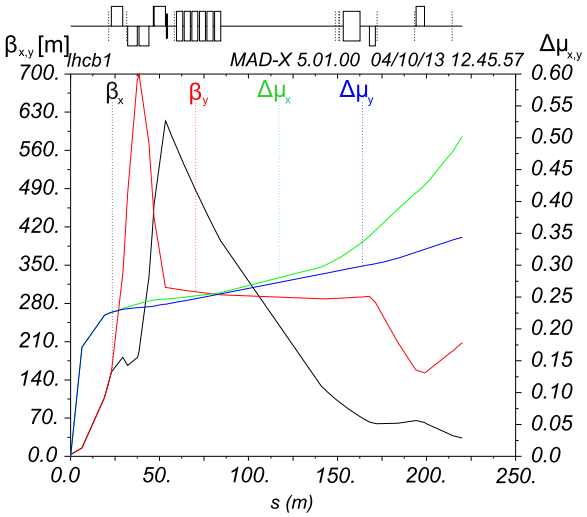

Figure 2. The horizontal β_x and vertical betatron amplitude β_y for the LHC $\beta^* = 3.5$ m optics. The horizontal μ_x and vertical phase advance μ_y are also shown, these functions are normalized to 2π. The plot shows that the horizontal phase advance $\Delta\mu_x = \pi$ close to the far RP unit.

Table 1. Sensitivity of the vertical effective length $L_{y,\,b_1}$ and $\mathrm{d}L_{x,\,b_1}/\mathrm{d}s$ to 1‰ deviations of magnet strengths or beam momentum for low- and high-β^*optics of the LHC beam 1. The total sensitivity to the perturbations of the quadrupole magnets' transverse position (Δx, $\Delta y = 1$ mm) and rotation ($\Delta\phi = 1$ mrad) is also included. The subscript b_1 indicates beam 1.

	$\delta L_{y,\,b_1,\,\mathrm{far}}/L_{y,\,b_1,\,\mathrm{far}}$ (%)		$\delta\left(\frac{\mathrm{d}L_{x,\,b1}}{\mathrm{d}s}\right)\Big/\frac{\mathrm{d}L_{x,\,b1}}{\mathrm{d}s}$ (%)	
Perturbed element	$\beta^* = 3.5$ m	$\beta^* = 90$ m	$\beta^* = 3.5$ m	$\beta^* = 90$ m
MQXA.1R5	0.98	0.14	−0.46	−0.42
MQXB.A2R5	−2.24	−0.24	0.33	0.31
MQXB.B2R5	−2.42	−0.25	0.45	0.42
MQXA.3R5	1.45	0.20	−1.14	−1.08
MQY.4R5.B1	−0.10	−0.01	−0.02	0.00
MQML.5R5.B1	0.05	0.04	0.05	0.06
$\Delta p_{b_1}/p_{b_1}$	−2.19	0.01	−0.79	0.71
$\Delta\phi_{\mathrm{quadrupoles}}$	0.01	3×10^{-3}	0.01	0.01
$(\Delta x,\,\Delta y)_{\mathrm{quadrupoles}}$	6×10^{-6}	1×10^{-5}	3×10^{-5}	2×10^{-5}
Total sensitivity	4.33	0.43	1.57	1.46

$$\Theta_y^* \approx \frac{y}{L_y}, \qquad \Theta_x^* \approx \frac{1}{\frac{\mathrm{d}L_x}{\mathrm{d}s}}\left(\Theta_x - \frac{\mathrm{d}v_x}{\mathrm{d}s}x^*\right), \quad x^* = \frac{x}{v_x}. \tag{7}$$

The vertical effective length L_y and the horizontal magnification v_x are applied in (7) due to their sizeable values, shown in figures 4 and 5. As the values of the reconstructed angles are

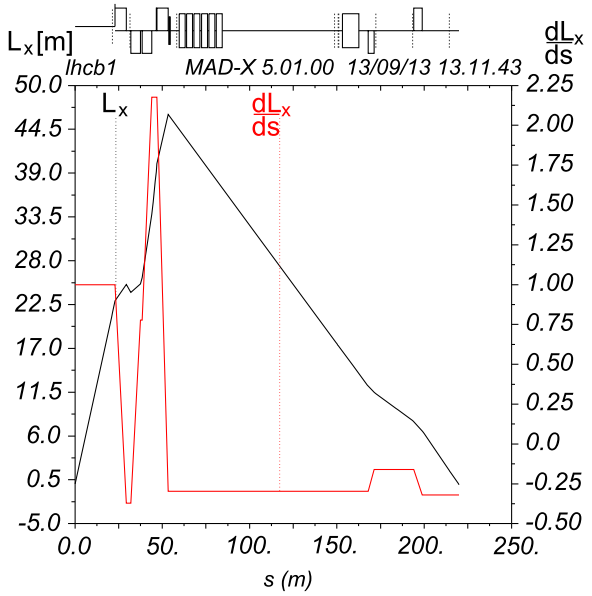

Figure 3. The horizontal effective length L_x and its derivative $\mathrm{d}L_x/\mathrm{d}s$ with respect to s as a function of the distance s in case of the LHC $\beta^* = 3.5$ m optics. The evolution of the optical functions is shown starting from IP5 up to the Roman pot stations. The plot indicates that $L_x = 0$ close to the far RP unit, thus in the proton kinematics reconstruction $\mathrm{d}L_x/\mathrm{d}s$ is used instead of L_x.

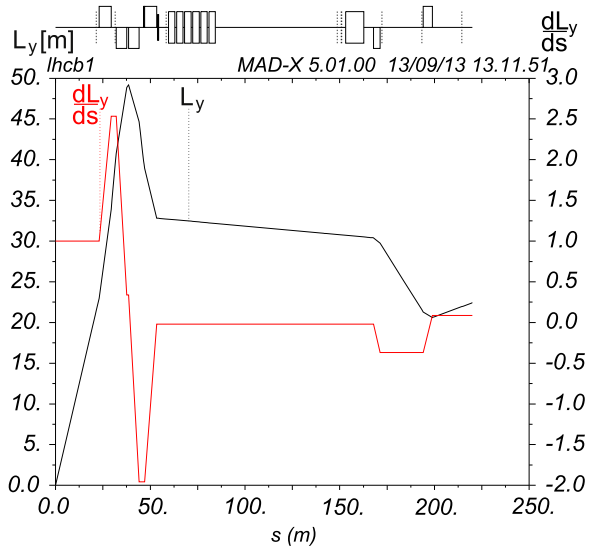

Figure 4. The evolution of the vertical effective length L_y and its derivative $\mathrm{d}L_y/\mathrm{d}s$ for the LHC $\beta^* = 3.5$ m optics between IP5 and the location of the Roman pot stations.

inversely proportional to the optical functions, the errors of the optical functions dominate the systematic errors of the final physics results.

The proton transport matrix $T(s; \mathcal{M})$, calculated with MAD-X [15], is defined by the machine settings $\mathcal{M}$, which are obtained on the basis of several data sources. The version V6.5

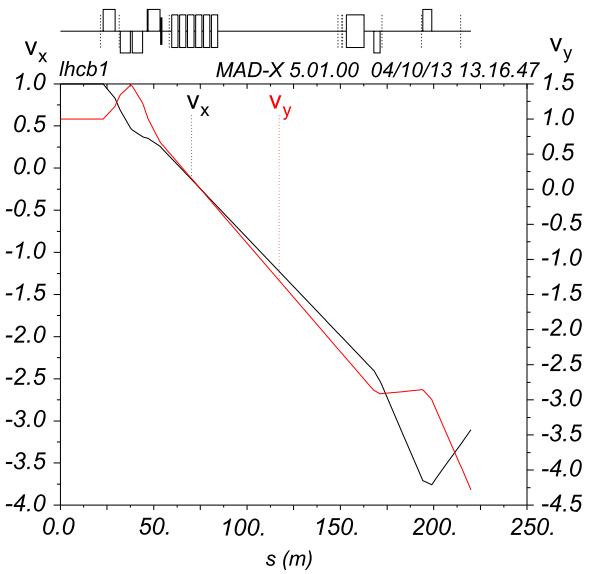

Figure 5. The evolution of the horizontal ν_x and vertical magnification ν_y in case of the LHC $\beta^* = 3.5$ m optics.

of the LHC sequence is used to describe the magnet lattice, while the nominal magnet strength file for a given beam optics is always updated using measured data: the currents of the magnet's power converters are first retrieved using TIMBER [16], which is an application to extract data from heterogeneous databases containing information about the whole LHC infrastructure.

Then the currents are converted to magnet strengths with the LHC software architecture [17] which employs for this purpose the conversion curves described by the field description for the LHC (FIDEL) [18].

The WISE database [20] contains the imperfections (field harmonics, magnets displacement, rotations) included in $\mathcal{M}$, as well as statistical models describing the non-measured parameters' tolerances. Alignment uncertainties of the magnets are included by WISE based on measurements of the mechanical and magnetic axes. Other uncertainties for example relative and absolute measurement errors of hysteresis and power converters accuracy are also included for all magnets.

3. Machine imperfections

The real LHC machine [2] is subject to additional imperfections $\Delta\mathcal{M}$, not measured well enough so far, which alter the transport matrix by ΔT:

$$T(s;\ \mathcal{M}) \to T(s;\ \mathcal{M} + \Delta\mathcal{M}) = T(s;\ \mathcal{M}) + \Delta T. \tag{8}$$

The most important are:

— magnet current-strength conversion error: $\sigma(k)/k \approx 10^{-3}$

— beam momentum offset: $\sigma(p)/p \approx 10^{-3}$.

Their impact on the most relevant optical functions L_y and $\mathrm{d}L_x/\mathrm{d}s$ can be calculated with MAD-X, the results are presented in table 1. It is clearly visible that the imperfections of the

inner triplet (the so called MQXA and MQXB magnets) are of high influence on the transport matrix while the optics is less sensitive to the strength of the quadrupoles MQY and MQML.

Other imperfections that are of lower, but not negligible, significance:

— magnet rotations: $\delta\phi \approx 1\,\mathrm{mrad}$
— beam harmonics: $\delta B/B \approx 10^{-4}$
— power converter errors: $\delta I/I \approx 10^{-4}$
— magnet positions: δx, $\delta y \approx 100\,\mu\mathrm{m}$.

Generally, as indicated in table 1, the low-β^* optics sensitivity to the machine imperfections is significant and cannot be neglected. For high-β^* optics the magnitude of ΔT is smaller in the vertical plane but in the horizontal plane the $\beta^* = 3.5$ m and $\beta^* = 90$ m optics result is similar. Due to the sensitivity of L_x the $\beta^* = 90$ m optics is also investigated in the following sections.

The proton reconstruction is based on (7). Thus it is necessary to know the effective lengths $L_{x,y}$ and their derivatives with an uncertainty better than 1–2% in order to measure the total cross-section σ_{tot} with the aimed uncertainty of [21]. The currently available $\Delta\beta/\beta$ beating measurement with an error of 5–10% does not allow us to estimate ΔT with the uncertainty, required by the TOTEM physics program [19, 22]. However, as it is shown in the following sections, ΔT can be determined well enough from the proton tracks in the Roman pots, by exploiting the properties of the optics and those of the elastic pp scattering.

4. Correlations in the transport matrix

The transport matrix T defining the proton transport from IP5 to the RPs is a product of matrices describing the magnetic field of the lattice elements along the proton trajectory. The imperfections of the individual magnets alter the cumulative transport function. It turns out that independently of the origin of the imperfection (strength of any of the magnets, beam momentum offset) the transport matrix is altered in a similar way, as can be described quantitatively with eigenvector decomposition, discussed in section 4.1.

4.1. Correlation matrix of imperfections

Assuming that the imperfections discussed in section 2 are independent, the covariance matrix describing the relations among the errors of the optical functions can be calculated

$$V = \mathrm{Cov}(\Delta T_r) = E\left(\Delta T_r \Delta T_r^T\right), \tag{9}$$

where T_r is the most relevant eight-dimensional subset of the transport matrix

$$T_r^{\mathrm{T}} = \left(v_x,\, L_x,\, \frac{\mathrm{d}v_x}{\mathrm{d}s},\, \frac{\mathrm{d}L_x}{\mathrm{d}s},\, v_y,\, L_y,\, \frac{\mathrm{d}v_y}{\mathrm{d}s},\, \frac{\mathrm{d}L_y}{\mathrm{d}s}\right), \tag{10}$$

which is presented as a vector for simplicity.

The optical functions contained in T_r differ by orders of magnitude and, are expressed in different physical units. Therefore, a normalization of V is necessary and the use of the correlation matrix C, defined as

$$C_{i,j} = \frac{V_{i,\,j}}{\sqrt{V_{i,\,i} \times V_{j,\,j}}}\,, \tag{11}$$

is preferred. An identical behaviour of uncertainties for both beams was observed and therefore it is enough to study the beam 1. In case of the $\beta^* = 3.5\,\mathrm{m}$ optics the following error correlation matrix is obtained using the MAD-X results of section 3:

$$C = \begin{pmatrix} 1.00 & 0.74 & -0.42 & -0.80 & -0.51 & -0.46 & -0.61 & -0.44 \\ 0.74 & 1.00 & -0.63 & -1.00 & -0.25 & -0.30 & -0.32 & -0.29 \\ -0.42 & -0.63 & 1.00 & 0.62 & 0.03 & 0.07 & 0.01 & 0.08 \\ -0.80 & -1.00 & 0.62 & 1.00 & 0.29 & 0.33 & 0.37 & 0.32 \\ -0.51 & -0.25 & 0.03 & 0.29 & 1.00 & 0.99 & 0.98 & 0.98 \\ -0.46 & -0.30 & 0.07 & 0.33 & 0.99 & 1.00 & 0.96 & 1.00 \\ -0.61 & -0.32 & 0.01 & 0.37 & 0.98 & 0.96 & 1.00 & 0.95 \\ -0.44 & -0.29 & 0.08 & 0.32 & 0.98 & 1.00 & 0.95 & 1.00 \end{pmatrix}. \tag{12}$$

The non-diagonal elements of C, which are close to ± 1, indicate strong correlations between the elements of ΔT_r. Consequently, the machine imperfections alter *correlated* groups of optical functions.

This observation can be further quantified by the eigenvector decomposition of C, which yields the following vector of eigenvalues $\lambda(C)$ for the $\beta^* = 3.5\,\mathrm{m}$ optics

$$\lambda(C) = (4.9,\ 2.3,\ 0.53,\ 0.27,\ 0.01,\ 0.01,\ 0.00,\ 0.00). \tag{13}$$

Since the two largest eigenvalues $\lambda_1 = 4.9$ and $\lambda_2 = 2.3$ dominate the others, the correlation system is practically two dimensional with the following two eigenvectors

$$v_1 = (0.35,\ 0.30,\ -0.16,\ -0.31,\ -0.40,\ -0.41,\ -0.41,\ -0.40), \tag{14}$$

$$v_2 = (-0.26,\ -0.46,\ 0.47,\ 0.45,\ -0.29,\ -0.27,\ -0.25,\ -0.28). \tag{15}$$

Therefore, contributions of the individual lattice imperfections cannot be evaluated. On the other hand, as the imperfections alter approximately only a two-dimensional subspace, a measurement of a small set of weakly correlated optical functions would theoretically yield an approximate knowledge of ΔT_r.

4.2. Error estimation of the method

Let us assume for the moment that we can precisely reconstruct the contributions to ΔT_r of the two most significant eigenvectors while neglecting the others. The error of such reconstructed transport matrix can be estimated by evaluating the contribution of the remaining eigenvectors:

$$\delta\Delta T_{r,\,i} = \sqrt{E_{i,\,i} \times V_{i,\,i}}\,, \tag{16}$$

Table 2. Nominal values of the optical functions $T_{r,i}$ and their relative uncertainty before ($\sqrt{V_{i,\,i}}/|T_{r,\,i}|$) and after ($\delta\Delta T_{r,\,i}/|T_{r,\,i}|$) the determination of the two most significant eigenvectors ($\beta^* = 3.5$ m, beam 1).

	$v_{x,\,\mathrm{far}}$	$L_{x,\,\mathrm{far}}$	$\frac{\mathrm{d}v_x}{\mathrm{d}s}$	$\frac{\mathrm{d}L_x}{\mathrm{d}s}$
$T_{r,\,i}$	-3.1	-1.32×10^{-1} m	3.1×10^{-2} m^{-1}	-3.21×10^{-1}
$\frac{\sqrt{V_{i,\,i}}}{\lvert T_{r,\,i}\rvert}$ (%)	2.0×10^{-1}	3.4×10^{2}	4.2×10^{-1}	1.6
$\frac{\delta\Delta T_{r,\,i}}{\lvert T_{r,\,i}\rvert}$ (%)	9.5×10^{-2}	9.1×10^{1}	2.6×10^{-1}	3.4×10^{-1}
	$v_{y,\,\mathrm{far}}$	$L_{y,\,\mathrm{far}}$	$\frac{\mathrm{d}v_y}{\mathrm{d}s}$	$\frac{\mathrm{d}Ly}{\mathrm{d}s}$
$T_{r,\,i}$	-4.3	2.24×10^{1} m	-6.1×10^{-2} m^{-1}	8.60×10^{-2}
$\frac{\sqrt{V_{i,\,i}}}{\lvert T_{r,\,i}\rvert}$ (%)	6.8×10^{-1}	4.3	5.9×10^{-1}	1.5×10^{1}
$\frac{\delta\Delta T_{r,\,i}}{\lvert T_{r,\,i}\rvert}$ (%)	6.1×10^{-2}	6.4×10^{-1}	8.3×10^{-2}	2.75

where

$$E = N \cdot \begin{pmatrix} 0 & 0 & 0 & 0 & 0 \\ 0 & 0 & 0 & 0 & 0 \\ 0 & 0 & \lambda_3 & 0 & 0 \\ \vdots & & & \ddots & \vdots \\ 0 & 0 & 0 & 0 & \lambda_8 \end{pmatrix} \cdot N^{\mathrm{T}} \tag{17}$$

and $N = (\nu_1, ..., \nu_8)$ is the basis change matrix composed of eigenvectors ν_i corresponding to the eigenvalues λ_i.

The relative optics uncertainty before and after the estimation of the most significant eigenvectors is summarized in table 2. According to the table, even if we limit ourselves only to the first two most significant eigenvalues, the uncertainty of optical functions due to machine imperfections drops significantly. In particular, in case of $\mathrm{d}L_x/\mathrm{d}s$ and L_y a significant error reduction down to a per mil level is observed. Unfortunately, due to $\Delta\mu_x = \pi$ (figure 2), the uncertainty of L_x, although importantly improved, remains very large and the use of $\mathrm{d}L_x/\mathrm{d}s$ for proton kinematics reconstruction should be preferred.

In the following sections a practical numerical method of inferring the optics from the RP proton tracks is presented and its validation with Monte Carlo calculations is reported.

5. Optics estimators from proton tracks measured by Roman pots ($\beta^* = 3.5$ m optics)

The TOTEM experiment can select the elastically scattered protons with high purity and efficiency [8, 9]. The RP detector system, due to its high resolution ($\sigma(x, y) \approx 11\,\mu$m, $\sigma(\Theta_{x,\,y}) \approx 2.9\,\mu$rad), can measure very precisely the proton angles, positions and the angle-position relations on an event-by-event basis. These quantities can be used to define a set of

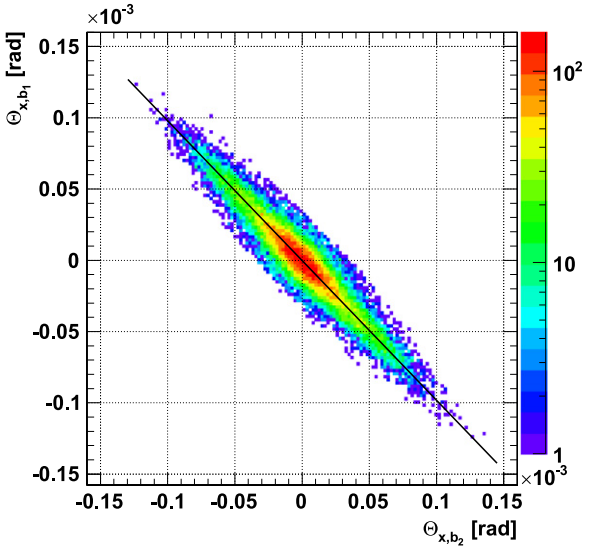

Figure 6. Beams 1 and 2 elastic scattering angle correlation in the horizontal plane $(\Theta_{x,b_1}, \Theta_{x,b_2})$ of protons detected by the Roman pots. The plot also illustrates the linear fit of the distribution whose slope parameter is the estimator $\hat{R}_1$.

estimators characterizing the correlations between the elements of the transport matrix T or between the transport matrices of the two LHC beams. Such a set of estimators $\hat{R}_1,...,\hat{R}_{10}$ (defined in the next sections) is exploited to reconstruct, for both LHC beams, the transport matrix $T(\mathcal{M}) + \Delta T$ defined in (8).

5.1. Correlations between the beams

Since the momentum of the two LHC beams is identical, the elastically scattered protons will be deflected symmetrically from their nominal trajectories of beams 1 and 2

$$\Theta^*_{x,\,b_1} = -\Theta^*_{x,\,b_2},\ \Theta^*_{y,\,b_1} = -\Theta^*_{y,\,b_2}, \tag{18}$$

which allows us to compute ratios $R_{1,2}$ relating the effective lengths at the RP locations of the two beams. From (1) and (18) we obtain

$$R_1 \equiv \frac{\Theta_{x,b_1}}{\Theta_{x,b_2}} \approx \frac{\frac{\mathrm{d}L_{x,b1}}{\mathrm{d}s} \times \Theta^*_{x,\,b_1}}{\frac{\mathrm{d}L_{x,b2}}{\mathrm{d}s} \times \Theta^*_{x,\,b_2}} = -\frac{\frac{\mathrm{d}L_{x,b1}}{\mathrm{d}s}}{\frac{\mathrm{d}L_{x,b2}}{\mathrm{d}s}}, \tag{19}$$

$$R_2 \equiv \frac{y_{b_1,\,\mathrm{far}}}{y_{b_2,\,\mathrm{far}}} \approx -\frac{L_{y,b_1,\,\mathrm{far}}}{L_{y,b_2,\,\mathrm{far}}}, \tag{20}$$

where the subscripts b_1 and b_2 indicate beams 1 and 2, respectively. Approximations present in (19) and (20) represent the impact of statistical effects such as detector resolution, beam divergence, primary vertex position distribution and longitudinal momentum spread of the particles. The estimators $\hat{R}_1$ and $\hat{R}_2$ are finally obtained from the $(\Theta_{x,\,b_1}, \Theta_{x,\,b_2})$ and $(y_{b_1,\,\mathrm{far}}, y_{b_2,\,\mathrm{far}})$ distributions and are defined with the help of the distributions' principal eigenvector, as illustrated in figures 6 and 7. The width of the distributions is determined by the

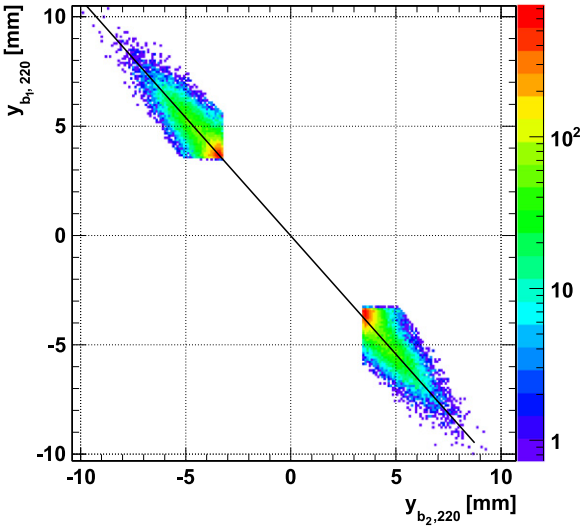

Figure 7. Correlation between positions (vertical projections) of elastically scattered protons detected in beams 1 and 2. The sharp edges are due to the vertical acceptance limits of the detectors. The plot also illustrates the linear fit of the distribution whose slope parameter is the estimator $\hat{R}_2$.

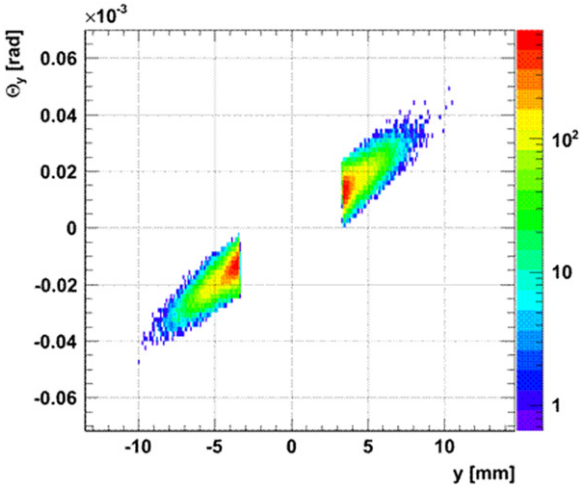

Figure 8. Correlation between vertical position and angle of elastically scattered protons at the RP of beam 1. This correlation plot illustrates the distribution which determines the estimator $\hat{R}_3$ and the corresponding plot of beam 2 is used for $\hat{R}_4$.

beam divergence and the vertex contribution, which leads to 0.5% uncertainty on the eigenvector's slope parameter.

5.2. Single beam correlations

The distributions of proton angles and positions measured by the Roman pots define the ratios of certain elements of the transport matrix T, defined by (1) and (2). First of all, $\mathrm{d}L_y/\mathrm{d}s$ and L_y are related by

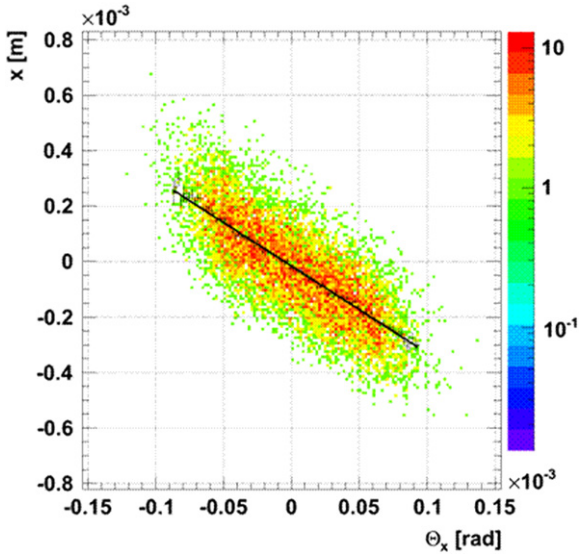

Figure 9. Correlation between the horizontal angle and position of elastically scattered protons at the RP of beam 1. The plot also illustrates the linear fit of the distribution whose slope parameter is the estimator $\hat{R}_5$ and the corresponding plot of beam 2 is used to determine $\hat{R}_6$.

$$R_3 \equiv \frac{\Theta_{y,\,b_1}}{y_{b_1}} \approx \frac{\frac{\mathrm{d}L_{y,\,b1}}{\mathrm{d}s}}{L_{y,\,b_1}}, \quad R_4 \equiv \frac{\Theta_{y,\,b_2}}{y_{b_2}} \approx \frac{\frac{\mathrm{d}L_{y,\,b2}}{\mathrm{d}s}}{L_{y,\,b_2}}. \tag{21}$$

The corresponding estimators $\hat{R}_3$ and $\hat{R}_4$ can be calculated with an uncertainty of 0.5% from the distributions as presented in figure 8.

Similarly, we exploit the horizontal dependencies to quantify the relations between $\mathrm{d}L_x/\mathrm{d}s$ and L_x. As L_x is close to 0, see figure 3, instead of defining the ratio we rather estimate the position s_0 along the beam line (with the uncertainty of about 1 m), for which $L_x = 0$. This is accomplished by resolving

$$\frac{L_x(s_0)}{\mathrm{d}L_x(s_1)/\mathrm{d}s} = \frac{L_x(s_1)}{\mathrm{d}L_x(s_1)/\mathrm{d}s} + (s_0 - s_1) = 0, \tag{22}$$

for s_0, where s_1 denotes the coordinate of the Roman pot station along the beam with respect to IP5. Obviously, $\mathrm{d}L_x(s)/\mathrm{d}s$ is constant along the RP station as no magnetic fields are present at the RP location. The ratios $L_x(s_1)\Big/\frac{\mathrm{d}L_x(s_1)}{\mathrm{d}s}$ for beams 1 and 2, similarly to the vertical constraints R_3 and R_4, are defined by the proton tracks

$$\frac{L_x}{\frac{\mathrm{d}L_x}{\mathrm{d}s}} \approx \frac{x}{\Theta_x}, \tag{23}$$

which is illustrated in figure 9. In this way two further constraints and the corresponding estimators (for beams 1 and 2) are obtained

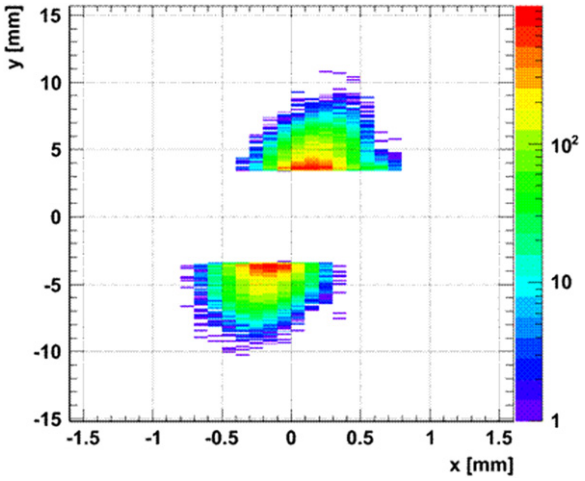

Figure 10. Vertical versus horizontal track position at the near RP of the LHC beam 1. This correlation plot illustrates the distribution which determines the estimator $\hat{R}_7$. The plot at the far RP is used to calculate $\hat{R}_8$ and the corresponding two plots of beam 2 is used for $\hat{R}_9$ and $\hat{R}_{10}$.

$$R_5 \equiv s_{b_1} \quad \text{and} \quad R_6 \equiv s_{b_2}. \tag{24}$$

5.3. Coupling / rotation

In reality the coupling coefficients $m_{13},...,m_{42}$ cannot be always neglected, as it is assumed by (6). RP proton tracks can help to determine the coupling components of the transport matrix T as well, where it is especially important that L_x is close to zero at the RP locations. Always based on (1) and (2), four additional constraints (for each of the two LHC beams and for each unit of the RP station) can be defined

$$R_{7,\,...,\,10} \equiv \frac{x_{\text{near(far)}}}{y_{\text{near(far)}}} \approx \frac{m_{14,\text{ near (far)}}}{L_{y,\text{ near (far)}}}. \tag{25}$$

The subscripts 'near' and 'far' indicate the position of the RP along the beam with respect to the IP. Geometrically $R_{7,\,...,\,10}$ describe the rotation of the RP scoring plane about the beam axis. Analogously to the previous sections, the estimators $\hat{R}_{7,\,...,\,10}$ are obtained from track distributions as presented in figure 10 and an uncertainty of 3% is achieved.

6. Optical functions estimation

The machine imperfections $\Delta\mathcal{M}$, leading to the transport matrix change ΔT, are in practice determined with the χ^2 minimization procedure:

$$\widehat{\Delta\mathcal{M}} = \arg\min\left(\chi^2\right), \tag{26}$$

defined on the basis of the estimators $\hat{R}_1,...,\hat{R}_{10}$, where the arg min function gives the phase space position where the χ^2 is minimized. As it was discussed in section 4.1, although the overall alteration of the transport matrix ΔT can be determined precisely based on a few optical

Table 3. Selected optical functions of both LHC beams for the $\beta^* = 3.5$ m and 90 m optics, obtained with the estimation procedure, compared to their nominal values.

$\beta^* = 3.5$ m				
	$L_{y,\,b_1,\,\mathrm{far}}$ (m)	$\mathrm{d}L_{x,\,b_1}/\mathrm{d}s$	$L_{y,\,b_2,\,\mathrm{far}}$ (m)	$\mathrm{d}L_{x,\,b_2}/\mathrm{d}s$
Nominal	22.4	-3.21×10^{-1}	18.4	-3.29×10^{-1}
Estimated	22.6	-3.12×10^{-1}	20.7	-3.15×10^{-1}
$\beta^* = 90$ m				
	$L_{y,\,b_1,\,\mathrm{far}}$ (m)	$\mathrm{d}L_{x,\,b_1}/\mathrm{d}s$	$L_{y,\,b_2,\,\mathrm{far}}$ (m)	$\mathrm{d}L_{x,\,b_2}/\mathrm{d}s$
Nominal	263.2	-5.36×10^{-1}	263.2	-5.36×10^{-1}
Estimated	264.1	-5.25×10^{-1}	266.3	-5.17×10^{-1}

functions' measurements, the contributions of individual imperfections cannot be established. In terms of optimization, such a problem has no unique solution and additional constraints, defined by the machine tolerance, have to be added.

Therefore, the χ^2 function is composed of the part defined by the Roman pot tracks' distributions and the one reflecting the LHC tolerances

$$\chi^2 = \chi^2_{\mathrm{Design}} + \chi^2_{\mathrm{Measured}}. \tag{27}$$

The design part

$$\chi^2_{\mathrm{Design}} = \sum_{i=1}^{12}\left(\frac{k_i - k_{i,\,\mathrm{MAD-X}}}{\sigma\left(k_i\right)}\right)^2 + \sum_{i=1}^{12}\left(\frac{\phi_i - \phi_{i,\,\mathrm{MAD-X}}}{\sigma\left(\phi_i\right)}\right)^2 + \sum_{i=1}^{2}\left(\frac{p_i - p_{i,\,\mathrm{MAD-X}}}{\sigma\left(p_i\right)}\right)^2, \tag{28}$$

where k_i and ϕ_{i} are the nominal strength and rotation of the ith magnet, respectively. Thus (28) defines the nominal machine $(k_i,\ \phi_i,\ p_i)$ as an attractor in the phase space. Both LHC beams are treated simultaneously. Only the relevant subset of machine imperfections $\Delta\mathcal{M}$ was selected. The obtained 26-dimensional optimization phase space includes the magnet strengths (12 variables), rotations (12 variables) and beam momentum offsets (two variables). Magnet rotations are included into the phase space, otherwise only the coupling coefficients $m_{13},\ \ldots,\ m_{42}$ could induce rotations in the (x, y) plane (25), which could bias the result.

The measured part

$$\chi^2_{\mathrm{Measured}} = \sum_{i=1}^{10}\left(\frac{\hat{R}_i - R_{i,\,\mathrm{MAD-X}}}{\sigma\left(\hat{R}_i\right)}\right)^2 \tag{29}$$

contains the track-based estimators $\hat{R}_1, \ldots, \hat{R}_{10}$ (discussed in detail in section 5) together with their uncertainty. The subscript 'MAD-X' defines the corresponding values evaluated with the MAD-X software during the χ^2 minimization.

Table 3 presents the results of the optimization procedure for the $\beta^* = 3.5\,\mathrm{m}$ optics used by LHC in October 2010 at beam energy $E = 3.5\,\mathrm{TeV}$. The obtained value of the effective length L_y of beam 1 is close to the nominal one, while beam 2 shows a significant change. The same pattern applies to the values of $\mathrm{d}L_x/\mathrm{d}s$. The error estimation of the procedure is discussed in section 7. The $\beta^* = 90\,\mathrm{m}$ results at $E = 4\,\mathrm{TeV}$ are also presented in table 3.

6.1. Interplay between the detector alignment and the optics matching procedure

Alignment procedures are practically independent from the optics imperfections. The relative RP alignment within a single arm is obtained solely on the basis of local proton tracks, by means of top and bottom RP overlaps with the horizontal devices. This procedure does not involve any optics assumption and the optics has no influence on it.

The further alignment of the above system with respect to the beam is performed with RP distributions of elastically scattered protons. The key cuts of elastic proton tagging (collinearity of left–right arm protons) require no prior optics knowledge while for the remaining cuts an indicative nominal optics knowledge is sufficient as they show insensitivity to expected optics errors [10]. Furthermore, the alignment techniques applied in TOTEM [5] rely only on the hit distribution symmetries. Although the optics imperfections may change the RP hit distributions, their symmetries are preserved making the alignment procedure immune to optics imperfections.

The estimators $\hat{R}_1$, $\hat{R}_5$ and $\hat{R}_6$ are insensitive to misalignment. The $\hat{R}_2$, $\hat{R}_3$ and $\hat{R}_4$ constraints are, in principle, very sensitive to relative top-bottom RP misalignment. However, such misalignment is very precisely determined by means of the relative alignment procedure.

Finally, there is an interplay between the RP unit rotation misalignment and the optics x–y coupling due to rotation misalignments of the lattice magnets. The quadrupole rotation misalignments can induce an x–y coupling, which provokes a RP x–y scoring plane rotation, consider (25). For low-β^* optics $\beta^* = 3.5\,\mathrm{m}$) the uncertainty of this rotation is 35 mrad when nominal LHC uncertainties are applied. Compared to an expected 1 mrad rotation alignment uncertainty of a RP unit, the lattice related effect is clearly larger and can be estimated.

However, large-β^* optics is characterized by large insensitivity to quadrupole magnet rotation misalignments. For $\beta^* = 90\,\mathrm{m}$ the RP x–y scoring plane rotation uncertainty of 1.8 mrad is expected which is compatible to the alignment uncertainty. Therefore in this case lattice rotation imperfections cannot be distinguished from RP rotation misalignment.

7. Monte Carlo validation

In order to demonstrate that the proposed $\hat{R}_i$ optics estimators are effective the method was validated with Monte Carlo simulations.

In each Monte Carlo simulation the nominal machine settings $\mathcal{M}$ were altered with simulated machine imperfections $\Delta\mathcal{M}$ within their tolerances using Gaussian distributions. The simulated elastic proton tracks were used afterwards to calculate the estimators $\hat{R}_1,\ldots,\hat{R}_{10}$. The study included the impact of

— magnet strengths,

— beam momenta,

— magnet displacements, rotations and harmonics,

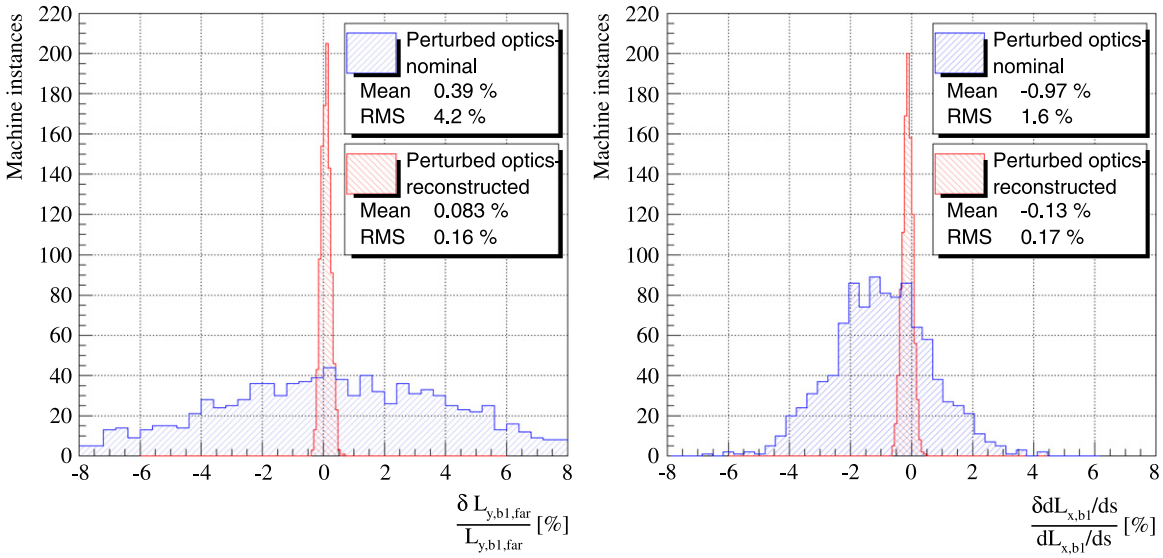

Figure 11. The MC error distribution of $\beta^* = 3.5$ m optical functions L_y and $\mathrm{d}L_x/\mathrm{d}s$ for beam 1 at $E = 3.5$ TeV, before and after optics estimation.

Table 4. The Monte Carlo study of the impact of the LHC imperfections $\Delta\mathcal{M}$ on selected transport matrix elements $\mathrm{d}L_x/\mathrm{d}s$ and L_y for $\beta^* = 3.5$ m at $E = 3.5$ TeV. The LHC parameters were altered within their tolerances. The relative errors of $\mathrm{d}L_x/\mathrm{d}s$ and L_y (mean value and rms) characterize the optics uncertainty before and after optics estimation.

	Simulated optics distribution		Reconstructed optics error	
Relative optics distribution	Mean (%)	rms (%)	Mean (%)	rms (%)
$\frac{\delta L_{y,\,b1,\,\mathrm{far}}}{L_{y,\,b1,\,\mathrm{far}}}$	0.39	4.2	8.3×10^{-2}	0.16
$\frac{\delta \mathrm{d}L_{x,\,b1}/\mathrm{d}s}{\mathrm{d}L_{x,b1}/\mathrm{d}s}$	−0.97	1.6	−0.13	0.17
$\frac{\delta L_{y,\,b2,\,\mathrm{far}}}{L_{y,\,b2,\,\mathrm{far}}}$	−0.14	4.9	0.21	0.16
$\frac{\delta \mathrm{d}L_{x,\,b2}/\mathrm{d}s}{\mathrm{d}L_{x,\,b2}/\mathrm{d}s}$	0.10	1.7	-9.7×10^{-2}	0.17

— settings of kickers,

— measured proton angular distribution.

The error distributions of the optical functions ΔT obtained for $\beta^* = 3.5$ m and $E = 3.5$ TeV are presented in figure 11 and table 4, while the $\beta^* = 90$ m results at $E = 4$ TeV are shown in figure 12 and table 5.

First of all, the impact of the machine imperfections $\Delta\mathcal{M}$ on the transport matrix ΔT, as shown by the MC study, is identical to the theoretical prediction presented in table 2. The bias

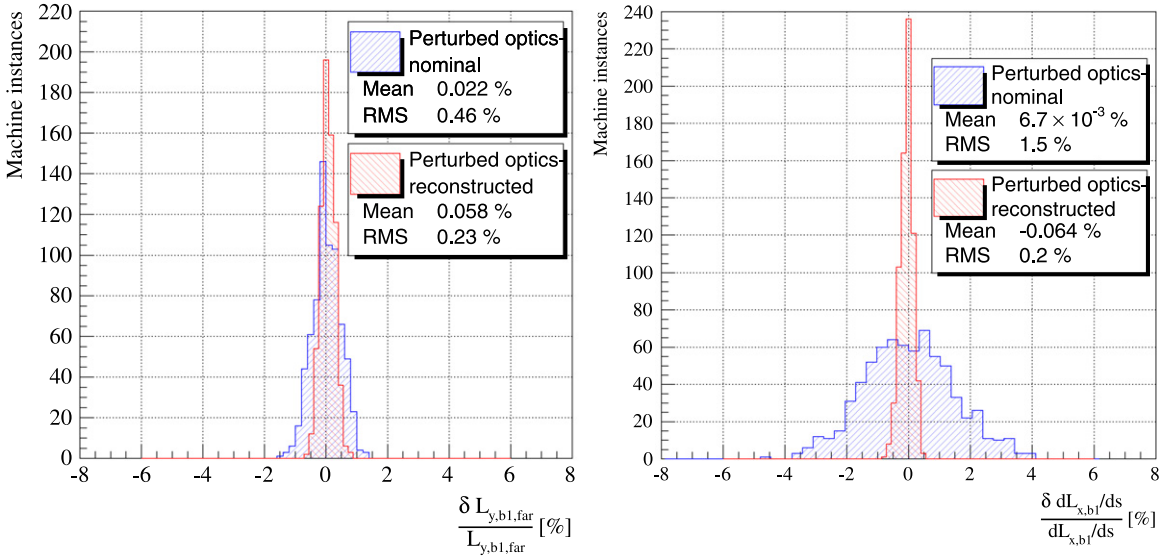

Figure 12. The MC error distribution of $\beta^* = 90$ m optical functions L_y and $\mathrm{d}L_x/\mathrm{d}s$ for beam 1 at $E = 4$ TeV, before and after optics estimation.

Table 5. The Monte-Carlo study of the impact of the LHC imperfections $\Delta\mathcal{M}$ on selected transport matrix elements $\mathrm{d}L_x/\mathrm{d}s$ and L_y for $\beta^* = 90$ m at $E = 4$ TeV. The LHC parameters were altered within their tolerances. The relative errors of $\mathrm{d}L_x/\mathrm{d}s$ and L_y (mean value and rms) characterize the optics uncertainty before and after optics estimation.

	Simulated optics distribution		Reconstructed optics error	
Relative optics distribution	Mean (%)	rms (%)	Mean (%)	rms (%)
$\frac{\delta L_{y,\,b1,\,\mathrm{far}}}{L_{y,b1,\,\mathrm{far}}}$	2.2×10^{-2}	0.46	5.8×10^{-2}	0.23
$\frac{\delta \mathrm{d}L_{x,\,b1}/\mathrm{d}s}{\mathrm{d}L_{x,\,b1}/\mathrm{d}s}$	6.7×10^{-3}	1.5	-6.4×10^{-2}	0.20
$\frac{\delta L_{y,\,b2,\,\mathrm{far}}}{L_{y,\,b2,\,\mathrm{far}}}$	-5×10^{-3}	0.47	5.8×10^{-2}	0.23
$\frac{\delta \mathrm{d}L_{x,\,b2}/\mathrm{d}s}{\mathrm{d}L_{x,\,b2}/\mathrm{d}s}$	1.8×10^{-2}	1.5	-7×10^{-2}	0.21

of the simulated optics distributions is due to magnetic field harmonics as reported by the LHC imperfections database [20]. The final value of mean after optics estimation procedure contributes to the total uncertainty of the method.

The errors of the reconstructed optical functions are significantly smaller than evaluated theoretically in section 4.2. This results from the larger number of constraints, design and measured constraints (27), employed in the numerical estimation procedure of section 6. In particular, the collinearity of elastically scattered protons was exploited in addition. Finally, the achieved uncertainties of $\mathrm{d}L_x/\mathrm{d}s$ and L_y are both lower than 2.5‰ for both beams.

8. Conclusions

TOTEM has proposed a novel approach to estimate the optics at LHC. The method, based on the correlations of the transport matrix, consists in the determination of the optical functions, which are strongly correlated to measurable combinations of the transport matrix elements.

At low-β^* LHC optics, where machine imperfections are more significant, the method allows us to determine the real optics with a per mil level of uncertainty, also permitting us to assess the transport matrix errors from the tolerances of various machine parameters. In the case of high-β^* LHC optics, where the machine imperfections have a smaller effect on the optical functions, the method remains effective and reduces the uncertainties to the desired per mil level. The method has been validated with the Monte Carlo studies both for high- and low-β^* optics and was successfully used in the TOTEM experiment to estimate the real optics for TOTEM physics runs.

Acknowledgments

This work was supported by the institutions listed on the front page and partially also by NSF (US), the Magnus Ehrnrooth foundation (Finland), the Waldemar von Frenckell foundation (Finland), the Academy of Finland, the Finnish Academy of Science and Letters (The Vilho, Yrjö and Kalle Väisälä Fund), the OTKA grant NK 101438 (Hungary) and the Ch. Simonyi Fund (Hungary).

References

[1] Antchev G *et al* 2008 *J. Instrum.* **3** S08007
[2] Evans L and Bryant P 2008 *J. Instrum.* **3** S08001
[3] Anelli G *et al* 2008 *J. Instrum.* **3** S08007
[4] Antchev G *et al* 2013 *Int. J. Mod. Phys.* A **28** 1330046
[5] Kašpar J 2011 *PhD Thesis* CERN-THESIS-2011-214
[6] Burkhardt H and White S 2010 *High-β^* Optics for the LHC* LHC Project Note 431
[7] Niewiadomski H 2008 *PhD Thesis* CERN-THESIS-2008-080
[8] Antchev G *et al* 2011 *Europhys. Lett.* **95** 41001
[9] Antchev G *et al* 2011 *Europhys. Lett.* **96** 21002
[10] Antchev G *et al* 2013 *Europhys. Lett.* **101** 21002
[11] Antchev G *et al* 2013 *Europhys. Lett.* **101** 21004
[12] Antchev G *et al* 2013 *Phys. Rev. Lett.* **111** 012001
[13] Wiedemann H 2007 *Particle Accelerator Physics* 3rd edn (Berlin: Springer) ISBN: 978-3540490432
[14] Evans L 2007 *New J. Phys.* **9** 335
[15] MAD-X: An upgrade from MAD8, CERN-AB-2003-024-ABP
[16] The LHC logging service, CERN-AB-Note-2006-046
[17] The LSA database to drive the accelerator settings, CERN-ATS-2009-100
[18] FIDEL—The Field Description for the LHC, LHC-C-ES-0012 ver.2.0
[19] β-beating in the effective model of the LHC using PTC CERN-ATS-Note-2011-096 TECH
[20] Hagen P *et al* 2008 WISE: A simulation of the LHC optics including magnet geometrical data *Proc. EPAC08 (Genova, Italy)*
[21] Berardi V *et al* 2004 *TOTEM Technical Design Report 1st edn (CERN, Geneva)* ISBN 9290832193.
[22] Tomás R *et al* 2010 LHC optics model measurements and corrections *Proc. IPAC10 (Kyoto, Japan)*